Suppression of autophagy dysregulates the antioxidant response and causes premature senescence of melanocytes.

Cheng-Feng Zhang[1,2], Florian Gruber[1,3], Chunya Ni[1,2], Michael Mildner[1], Ulrich Koenig[1], Susanne Karner[1], Caterina Barresi[1], Heidemarie Rossiter[1], Marie-Sophie Narzt, Ionela Mariana Nagelreiter, Lionel Larue[4,5,6], Desmond J. Tobin[7], Leopold Eckhart[1], Erwin Tschachler[1]

[1] Research Division of Biology and Pathobiology of the Skin, Department of Dermatology, Medical University of Vienna, Vienna, Austria

[2] Department of Dermatology, Huashan Hospital, Fu Dan University, Shanghai, China

[3] Christian Doppler Laboratory for Biotechnology of Skin Aging, Department of Dermatology, Medical University of Vienna, Vienna, Austria

[4] Institut Curie, Centre de Recherche, Developmental Genetics of Melanocytes, Orsay, France

[5] CNRS UMR3347, Orsay, France

[6] INSERM U1021, Orsay, France

[7] Centre for Skin Sciences, School of Life Sciences, University of Bradford, Bradford, West Yorkshire, United Kingdom

Correspondence: Erwin Tschachler, Department of Dermatology, Medical University of Vienna, Währinger Gürtel 18-20, Vienna A-1090, Austria. E-mail: Erwin.Tschachler@meduniwien.ac.at

Abbreviations: MC, melanocyte; KC, keratinocyte; NRF2, nuclear factor erythroid 2–related factor 2; LC3, microtubule-associated protein light chain 3; NQO1, NAD(P)H dehydrogenase, quinone 1; p62, p62/SQSTM1- sequestosome-1; p16, p16ink4a /CDKN2A; p21, CDKN1A; GCLM, γ-glutamyl cystine ligase modulatory subunit; GCLC, γ-glutamyl cystine ligase catalytic subunit; GSTM, glutathione S-transferase Mu 1; HO-1,HMOX1, heme oxygenase-1; Mitf, microphthalmia-associated transcription factor; qPCR, relative quantitative real-time PCR.

Abstract

Autophagy is the central cellular mechanism for delivering organelles and cytoplasm to lysosomes for degradation and recycling of their molecular components. To determine the contribution of autophagy to melanocyte (MC) biology, we inactivated the essential autophagy gene *Atg7* specifically in melanocytes using the Cre-loxP system. This gene deletion efficiently suppressed a key step in autophagy, lipidation of microtubule-associated protein 1 light chain 3 beta (LC3), in MC and induced slight hypopigmentation of epidermis in mice. The melanin content of hair was decreased by 10-15% in mice with autophagy-deficient MC as compared to control animals. When cultured *in vitro*, MC from mutant and control mice produced equal amounts of melanin per cell. However, *Atg7*-deficient MC entered into premature growth arrest and accumulated reactive oxygen species (ROS) damage, ubiquitinated proteins and the multi-functional adaptor protein SQSTM1/p62. Moreover, nuclear factor erythroid 2–related factor 2 (Nrf2)-dependent expression of NAD(P)H dehydrogenase, quinone 1 (Nqo1) and glutathione S-transferase Mu 1 (Gstm1) was increased, indicating a contribution of autophagy to redox homeostasis in MC. In summary, the results of our study suggest that *Atg7*-dependent autophagy is dispensable for melanogenesis but necessary for achieving the full proliferative capacity of MC.

Introduction

Autophagy is an evolutionarily conserved mechanism by which cells degrade and recycle their own structural components. It is critical for the removal of damaged proteins and subcellular organelles, the maintenance of cell metabolism during starvation, cellular remodeling during development and differentiation as well as anti-bacterial and anti-viral defense (Mizushima, 2007;Mizushima and Komatsu, 2011;Deretic, 2011). Macroautophagy is considered the predominant mode of autophagy in mammalian tissues (Mizushima and Komatsu, 2011) and will hereafter be referred to as "autophagy". Chaperone-mediated autophagy and microautophagy are alternative mechanisms of autophagy that mediate the degradation of different subcellular substrates in a largely non-redundant manner (Mizushima and Komatsu, 2011;Santambrogio and Cuervo, 2011). Autophagy is controlled by a defined set of gene products which have been reviewed previously (Yang and Klionsky, 2010;Mizushima and Levine, 2010). The ATG7 protein is essential for the conversion of the cytosolic form of microtubule-associated protein light chain 3 (LC3), LC3-I, into its lipidated form, LC3-II – an obligatory step of autophagy. LC3-II associates with isolation membranes to form autophagosomes and interacts with p62/SQSTM1, the adaptor protein that targets cargo for selective autophagosomal degradation. Inactivation of Atg7 disrupts autophagy by preventing lipidation of LC3 and thus autophagosome formation. Germline inactivation of Atg7 leads to perinatal lethality that correlates with decreased levels of amino acids compared to wild type mice in the neonatal starvation period (Komatsu *et al.*, 2005). Targeted inactivation of Atg7 in the central nervous system resulted in neurodegeneration and death 28 weeks after birth (Komatsu *et al.*, 2006); liver-targeted inactivation led to a massive hepatomegaly and accumulation of abnormal organelles in liver cells (Komatsu *et al.*, 2005).

Melanocytes (MC) are neural crest-derived pigment producing cells which migrate into the skin during embryogenesis and colonize the epidermis and hair follicles (Hearing, 1993;Luciani *et al.*, 2011). In mice MC are present in the epidermis at all body sites only around the time of birth (Hirobe, 1984). After the first postnatal week MC are mainly present within the dermis and the hair follicles in hairy skin whereas in ear and tail skin epidermal MC persist throughout adult life. Activated MC produce melanin which is transferred to differentiating hair keratinocytes and, on tail and ear skin, also to interfollicular keratinocytes (Slominski *et al.*, 2005). Proliferation, migration and differentiation of mouse MC during development are regulated by numerous genetic and epigenetic factors (Hirobe, 2011;Bonaventure *et al.*, 2013). siRNA-based screens identified autophagy genes as having an impact on melanogenesis and heterozygosity for the autophagy regulator beclin 1 resulted in altered fur color of mice (Ganesan *et al.*, 2008). In addition members of the autophagic machinery have been proposed to play a role in the

formation and maturation of melanosomes (Ho and Ganesan, 2011;Kim *et al.*, 2014), however, direct evidence for this claim is lacking.

Here, we investigated whether or not autophagy plays a role in melanogenesis and MC homeostasis. To this end, mice carrying a floxed Atg7 gene (Komatsu *et al.*, 2005) were crossed with mice expressing the Cre recombinase under the control of the tyrosinase promoter (Delmas *et al.*, 2003) which is active in neural crest–derived pigment cells. We demonstrate that the disruption of autophagy does not prevent melanogenesis although it leads to a slight but significant reduction of melanin content in both hair and tail epidermis. Cultured autophagy deficient MC showed a strongly reduced capacity to proliferate and became prematurely senescent. At the molecular level, the lack of autophagy was associated with the accumulation of p62/SQSTM1 both *in vivo* and *in vitro*, the up-regulation of nuclear factor E2–related factor 2 (Nrf2) signaling but also ROS and lipid oxidation. The results of this study suggest that Atg7-dependent autophagy is dispensable for melanogenesis but important for the control of the Nrf2 stress response and sustained proliferation of MC.

Results

Autophagy is constitutively active in normal human and murine melanocytes

To explore whether autophagy is active in MC, we investigated the effect of the classical autophagy inducer rapamycin on the lipidation status of LC3 in cultured normal human and murine MC by Western blot analysis. As shown in Figure 1, both human and murine MC already contained high levels of autophagy-associated, lipidated LC3-II (human 70% +/- 14% of total LC3, n=4; mouse 58% +/- 4%, n=3) in their basic state indicating that autophagy is constitutively active in MC *in vitro*. Addition of rapamycin to the culture medium caused only a slight additional increase of LC3-II in MC (human 74% +/- 23% and mouse 70% +/- 10 %, respectively , the latter induction being significant with $p < 0.05$).

Tyr::Cre-mediated deletion of Atg7 efficiently suppresses autophagy in melanocytes

To specifically inactivate the Atg7 gene in pigment cells, mice carrying a floxed allele of *Atg7* (Komatsu *et al.*, 2005) were mated to the Tyr::Cre mouse line, which triggers recombination in cells of the melanocyte lineage starting from 9.5 days of gestation (Puig *et al.*, 2009). Since the Tyr::Cre transgene is located on the X chromosome, hemizygous males and homozygous females were used as sources of MC for *in vitro* experiments. For *in vivo* analyses, only male Atg7 f/f (Xtg/Y) mice (here referred to as Atg7 f/f Tyr::Cre) were used in comparison to male Atg7 f/f (Xo/Y) mice (here referred to as Atg7 f/f). Efficient deletion of the floxed region of the Atg7 gene in MC isolated from Atg7 f/f Tyr::Cre mice was confirmed by PCR of genomic DNA (Figure 2a). Western blot analysis further confirmed that ATG7 protein was not produced in MC derived from ATG7 f/f Tyr::Cre animals (Figure 2b, uppermost panel). Functionally, the conversion of LC3-I to LC3-II was completely blocked in MC of ATG7 f/f Tyr::Cre mice, while bands of both LC3-I and LC3-II were readily detected in MC of Atg7 f/f mice (Figure 2b middle panel). Taken together, these data demonstrate that the autophagic machinery was efficiently disrupted in MC of Atg7 f/f Tyr::Cre mice.

Inactivation of ATG7-dependent autophagy in MC leads to decreased pigmentation of dorsal hair and tail epidermis in situ but does not affect the relative melanin content of cultured MC

Atg7 f/f Tyr::Cre mice were viable and as fertile as Atg7 f/f mice. The pigmentation of tail skin of Atg7 f/f Tyr::Cre mice was consistently lower than that of Atg7 f/f mice (Figure 3a) and to a lesser extent at the feet (not shown), whereas, by visual inspection, the coat color of Atg7 f/f Tyr::Cre mice was indistinguishable from that of Atg7 f/f mice. However, photometric quantification of melanin in extracts from shaved hair of the back showed that the melanin content of hair from Atg7 f/f Tyr::Cre mice was

about 10-15% lower than that of equally aged Atg7 f/f mice (Figure 3b, *p<0.05, **p<0.01). Melanocyte numbers per area were consistently but not sigificantly (p=0.1) lower in epidermis of autophagy deficient mice (Supplementary Figure S1)

Ultrastructural investigation by electron microscopy revealed that both MC and keratinocytes of tail skin contained mature melanosomes irrespectively of the presence of Atg7 in MC, strongly suggesting that autophagy is dispensable for melanosome formation, maturation and transfer (Supplementary Figure S2). Of note, some MC of mutant but not control mice contained misshapen, swollen and possibly disintegrating mitochondria.

When isolated and cultured *in vitro* autophagy-deficient and autophagy-competent MC contained similar amounts of melanin per cell (Figure 3c), and electron microscopy confirmed the presence of mature melanosomes (defined as fully electron dense granules reflective of high levels of melanin deposition) in cells of both genotypes (Supplementary Figure 1). However, mutant cells exhibited increased melanosome-associated vacuolation. The MC marker genes *Tyrosinase* and *Mitf* were expressed at comparable levels in both the absence and presence of autophagy, as determined by quantitative RT-PCR (data not shown). Taken together, these results indicate that MC need Atg7-dependent autophagy to achieve full pigmentation of hair and epidermis, but also that melanogenesis can proceed in the absence of an intact autophagy system.

Autophagy deficiency results in decreased proliferation and premature senescence of cultured MC

Next we characterized the impact of autophagy-deficiency on MC in cell cultures. MC derived from Atg7 f/f Tyr::Cre mice showed an altered growth profile as compared to MC from ATG7 f/f mice (Figure 4 a). In fact, Atg7 deficient MC stopped proliferation already after the third passage at around the fifth week in culture whereas normal MC continued proliferation and could be maintained up to passage 5. Analysis of Ki-67 expression on day 23 of culture confirmed that the proportion of proliferating cells was strongly decreased in cultures of Atg7 f/f Tyr::Cre MC (Figure 4 b, c). In addition mutant MC started to change their morphology early in the second passage at around week 3, and acquired senescent morphotypes with distended cytoplasms. The premature senescent phenotype became even more prominent at the end of passage 2 and beginning of passage 3 (Figure 4 d). By contrast, similar changes in cell morphology were observed in control MC only at around 9 weeks in culture, when the cells had been passaged five times. The changes in the morphology of autophagy-deficient MC were accompanied by significantly higher expression of p16Ink4a and p21 mRNAs (Figure 4 e, p<0.05), and a significantly higher proportion of mutant cells exhibited nuclear p16Ink4a protein as determined by immunofluorescence staining (Figure 4 f, g). Nuclear translocation of p16Ink4a (that has been reported (Piepkorn, 2000)) increased upon UVB

irradiation (20 mJ/cm²) in autophagy-competent cells whereas it could not be elevated above the high basal level in autophagy-deficient cells (Figure 4 f, g). Taken together these data suggest that the absence of autophagy leads to premature senescence of MC.

Autophagy deficiency leads to accumulation of high molecular weight protein aggregates containing p62/SQSTM1

Since autophagy controls several cellular processes via the modulation of distinct multifunctional proteins such as the cargo adaptor protein p62/SQSTM1 (Pankiv *et al.*, 2007), we determined the abundance of p62 and the activity of p62-related processes in normal and Atg7-deficient MC. As determined by Western blot analysis, the abundance of the autophagy substrate p62 was strongly increased in autophagy-deficient MC. Moreover, a massive accumulation of p62/SQSTM1- high molecular weight protein species was observed in lysates of autophagy-deficient MC indicative of p62 oligomerization (Kirkin *et al.*, 2009;Riley *et al.*, 2010) (Figure 5a). Double immune-labeling of cultured cells showed strongly increased levels of both p62/SQSTM1 and ubiquitinylated proteins in mutant MC (Figure 5b). In the cytoplasm, but not the nucleus these two proteins largely co-localized. Accumulation of p62/SQSTM1 also occurred also *in vivo* as demonstrated by double labeling of MC for p62/SQSTM1 and tyrosinase in epidermal sheet preparations of tail skin (Figure 5 c). The massive accumulation of p62/SQSTM1 protein was accompanied by an up-regulation of p62/SQSTM1 mRNA in cultured MC (Figure 5d) suggesting that not only a block in the degradation of the protein but also enhanced transcription contributed to the increase of p62/SQSTM1 protein in autophagy-deficient MC.

Persistently enhanced Nrf2 activity does not prevent increased ROS formation and lipid oxidation in autophagy deficient Melanocytes.

Accumulation of p62/SQSTM1 has potential to affect cell homeostasis via its crosstalk with the redox sensitive nuclear factor (erythroid-derived 2)-like 2 (Nrf2) signaling. p62/SQSTM1 is transcriptionally up-regulated by Nrf2, and in turn, accumulation of p62/SQSTM1 activates the Nrf2 signaling pathway in a positive feedback loop by competing with Nrf2 for binding to KEAP1 and favouring Nrf2 nuclear translocation (Komatsu et al., 2010). Suppression of autophagy results in Nrf2 dysregulation mainly upon UVA stress in cultured keratinocytes, (Zhao et al., 2013) and in a weak epidermal phenotype in vivo (Rossiter et al., 2013), whereas it causes severe dysregulation of Nrf2 in hepatic and pulmonary epithelial cells resulting in severe pathologic tissue damage (Inoue et al., 2011;Riley et al., 2010). Thus we investigated whether Nrf2 target genes were also induced in autophagy-deficient MC. qPCR analysis showed the canonical Nrf2 target genes NAD(P)H dehydrogenase quinone 1 (Nqo1), glutamate-cysteine ligase modifier subunit (Gclm) and glutathione S-transferase mu 1 (Gstm1) were expressed at significantly

higher levels in MC of mutant mice than in those of control animals (Figure 6a). By contrast, the heme oxygenase 1 (Hmox1) gene, which frequently is co-regulated with the aforementioned Nrf2 targets in keratinocytes (Zhao et al., 2013), was not significantly induced in autophagy-deficient MC, pointing to a cell type-specific control of Hmox1. Western blot analysis confirmed that also proteins encoded by distinct Nrf2 target genes, i.e. Gstm1 and Nqo1 were increased (Figure 6b). The expression of Nrf2 itself was weakly but not significantly increased by autophagy deficiency (Supplementary Figure 3), compatible with a model in which accumulating p62 would mediate increased translocation and activity of Nrf2, as found in other cases of autophagy deficiency(Komatsu *et al.*, 2010;Jain *et al.*, 2010;Ichimura *et al.*, 2013). Thus, by reducing the abundance of p62, autophagy would dampen Nrf2-dependent gene transcription in normal MC, whereas abrogation of homeostatic autophagy would trigger a persistent stress response. So we next investigated how the increased activation of Nrf2 and thus enhanced synthesis of oxidoreductases and cellular antioxidants would affect, in absence of autophagy, cellular ROS levels. To investigate differences in cellular ROS levels, we used a ROS sensitive probe (CellROX green) to determine differences in wild-type and Atg7 deficient melanoctes (MC) in tissue culture and found a significant increase in ROS in the Atg7 deficient MC. To assess biologically relevant consequences of ROS stress we measured with HPLC-MS-MS (Gruber et al., 2012) the levels of phospholipid hydroperoxides in autophagy competent and autophagy deficient cells as mechanistic reporter for oxidative stress (Girotti, 1998). The hydroperoxide oxidation products of the abundant phospholipids 1-stearoyl-2-linoleoyl-sn-glycero-3-phosphocholine (SLPC, 18:0-18:2 PC, *m/z* 786) and 1-palmitoyl-2-linoleoyl-sn-glycero-3-phosphocholine (PLPC, 16:0-18:2 PC, *m/z* 758) were significantly increased relative to their unoxidized precursors in lipid extracts from cultured autophagy deficient melanocytes, whereas the levels of unoxidized di-palmitoyl- sn-glycero-3-phosphocholine (DPPC, 16:0-16:0 PC *m/z* 734), was not significantly changed (Figure 6c). These data indicate that deficiency in autophagy, in addition to premature senescence, results in increased oxidative stress in melanocytes, despite the observed increase in Nrf2 activation.

Discussion

Proteins of the autophagic machinery, including beclin 1 (Funderburk *et al.*, 2010), ULK1 (Kalie *et al.*, 2013) and LC3-II have been previously suggested to participate in melanogenesis (Ganesan *et al.*, 2008), and autophagy has been hypothesized to participate also in melanosome formation and maturation (Ho and Ganesan, 2011). Here we have, for the first time, inactivated the central regulator of autophagy, Atg7, specifically in MC and studied pigmentation and MC homeostasis in transgenic mice and MC isolated from these mice. Our findings that mutant mice showed only a slight, although consistent, reduction of hair and skin pigmentation and that mutant melanocytes are able to produce mature melanosomes suggests that autophagy is neither essential for melanin production by MC nor for the delivery of melanin to hair and epidermal keratinocytes. Thus, the results of this study establish that, at least under standard animal care conditions, autophagy is not essential for MC survival and function *in vivo*.

When analyzing isolated MC in tissue culture we could confirm that the absence of autophagy did neither impact pigment production nor formation and maturation of melanosomes. Murase and coworkers, studying human cells in vitro, suggested recently that KC contribute to skin pigmentation by degrading melanosomes (Murase et al., 2013). As we have previously reported, mice deficient in KC autophagy did not show differences in skin or hair color (Rossiter et al., 2013) and in preliminary assessment of mice in which Atg7 was deleted in both MC and KC (Atg7 f/f Tyr::Cre, K14::cre) we found no differences with regard to coat and tail skin pigmentation to animals with autophagy-deficient MC only (not shown). Therefore a mechanism by which autophagy in KC contributes to skin color as suggested by Murase and coworkers (Murase et al., 2013), is not operant in vivo in mice. By contrast, autophagy deficient MC isolated from the skin of newborn mice differed considerably from autophagy competent MC in their proliferative capacity. In fact, Atg7-deficient MC virtually stopped proliferation during the 3rd passage *in vitro*, acquired a senescent morphology and expressed significantly higher levels of p16ink4 mRNA and proteins than control cells. This finding is in line with earlier reports which have shown that autophagy is involved in the regulation of the lifespan of cells (Vellai, 2009;Lionaki *et al.*, 2013). In cultured fibroblasts, senescence is associated with a decrease in the protein levels of S6K1, 4E-BP1, beclin-1, and Atg7 (Kang *et al.*, 2011) . In turn, the impairment of autophagy induces premature senescence, supposedly via mechanisms that involve aberrant oxidation of proteins accumulation of misfolded proteins and damaging levels of mitochondrial ROS (Sena and Chandel, 2012). Our finding that autophagy-deficient MC stopped proliferating and acquired a senescent phenotype earlier than their autophagy-competent counterparts provides support for a protective role of autophagy for the maintenance of the MC population. However, this *in vitro* finding does not translate into a statistically significant difference in the number of epidermal MC between mutant and control animals *in vivo*. In addition, the maintained pigmentation of

hair in aging mice showed that autophagy deficient MC were able to replenish hair follicles during the hair cycles throughout the lifespan of the animals. There are several possible explanations for the different effects of autophagy suppression *in vitro* and *in vivo*. In culture, the growth medium drives MC to continuous proliferation whereas *in vivo* MC proliferate mainly during the hair cycles(Slominski and Paus, 1993) and after UV exposure(van Schanke A. *et al.*, 2005). Continuous proliferation with increased metabolism in tissue culture might therefore result in an exhaustion of the cellular mechanisms that compensate for the absence of autophagy whereas such a state may not be reached *in vivo* during the normal life span of mice. Alternatively compensation for the lack of autophagy in MC *in vivo* might be provided by the surrounding tissue. That such a scenario is conceivable is hinted by a recent report on a breast cancer tumor model in which serum-starved mesenchymal stem cells activating autophagy supported tumor cell survival by paracrine mechanisms (Sanchez *et al.*, 2011). The recent finding that even aggregated proteins can be transferred to neighboring cells (Guo and Lee, 2014) even opens the possibility that autophagy-deficient MC may dispose of protein aggregates by delivering them to surrounding skin cells. Intriguingly, amyloid-like proteins are present in melanosomes and are consequently delivered to keratinocytes (Singh *et al.*, 2010). A potential dependence of autophagy-deficient MC on autophagy in neighboring skin cells will have to be addressed in separate studies.

In addition to the premature cessation of proliferation of autophagy deficient MC, we have here identified a significant dysregulation of a key stress response system of the cell, i.e. the Nrf2-dependent expression of anti-oxidant genes. Nrf2 provides adaptive cytoprotection against various ROS by inducing the expression of multiple antioxidant proteins and detoxifying enzymes (Kobayashi and Yamamoto, 2005). However, activation of Nrf2 signaling also requires tight control as evidenced by the observations that sustained high-level activity of Nrf2 in epidermal keratinocytes significantly disturbs tissue homeostasis (Schafer *et al.*, 2012). Hyperactivation of Nrf2 in autophagy deficient liver, brain and lung tissue (Riley et al., 2010;Inoue et al., 2011) results in deleterious damage that can be reverted by deleting Nrf2. Recently, a link between Nrf2 and autophagy was uncovered, as the autophagy cargo adaptor SQSTM1/p62 is both an activator of Nrf2 activity and an Nrf2 target gene (Komatsu *et al.*, 2010). In autophagy-deficient kidney and lung, SQSTM1/p62 accumulation in the cytoplasm, competes with Nrf2 for binding to its cytoplasmic anchor KEAP1 and thereby causes enhanced Nrf2 nuclear localization and transcription of its targets, one of them being SQSTM1/p62 itself. That this regulatory loop is indeed active in MC is strongly suggested by our finding that not only SQSTM1/p62 protein but also mRNA is increased in mutant MC. The Nrf2 pathway contributes to the regulation of the anti-oxidant response in MC (Marrot *et al.*, 2008), whereas Nrf2 signaling is downregulated after UVB irradiation in MC if not counteracted by alphaMSH(Kokot *et al.*, 2009). Our finding that autophagy deficient MC have increased expression levels of several Nrf2 target genes indicates aberrant activation of Nrf2 signaling in these cells. The repertoire of dysregulated

Nrf2 target genes seems to be determined by the cell type, as Hmox1, which is significantly induced in autophagy deficient KC is not overexpressed in autophagy deficient MC, and this asks for further investigation. The increased expression of cellular antioxidants does however not result in a reduction of ROS but rather an increase in phospholipid hydroperoxide levels as markers of oxidative stress. As we have observed earlier that also autophagy deficient keratinocytes display enhanced lipid oxidation (Zhao *et al.*, 2013), these findings strengthen the concept that functioning macroautophagy may contribute to removal or prevention of excess oxidized lipids. In case of the melanocytes, it can however not be ruled out that the oxidized lipids accumulate as result of beginning cellular senescence (Girotti and Kriska, 2004).

Our finding that autophagy-deficient melanocytes undergo premature senescence *in vitro* resembles what has been described for melanocytes from patients with vitiligo, therefore the role for autophagy in this disease deserves investigation: Not only do cultured melanocytes from vitiligo patients show signs of sublethal oxidative stress but they also present a pre-senescent phenotype, including increased expression and nuclear staining for p16 (Bellei et al., 2013), both strikingly similar to what we observed in autophagy deficient MC. The study by Bellei and another study by the same group (Dell'Anna et al., 2010) further described the detection of oxidzided membrane lipids in vitiligo MC. This again is comparable to the significant increase in oxidation products of two major membrane phospholipids which we detected in autophagy deficient cells. Finally, Nrf2 signalling is dysregulated in human vitiligo, and whereas high Nrf2 activation and expression of NQO1 and GCLM has been observed in lesional versus non-lesional epidermal samples form patients (Natarajan et al., 2010), it has been reported recently that vitiligo melanocytes cannot respond properly to oxidative stress and have an impaired heme oxygenase 1 response to hydrogen peroxide (Jian et al., 2014). Our findings are thus compatible with a model in which autophagy deficient MC and MC in vitiligo share an ineffective antioxidant defense, cellular redox dysregulation, increased membrane lipid oxidation and premature senescence. However, since autophagy only marginally affects pigmentation and melanocyte numbers in unchallenged mouse skin, we can at the present time neiter confirm nor exclude that dysregulated autophagy is relevant in vitiligo.

In conclusion our study challenges hypotheses that autophagy plays an essential role in melanogenesis or melanin delivery to KC but uncovers a crucial role of autophagy in the control of MC survival and proliferation. Moreover, the discovery of aberrant Nrf2 signaling in autophagy-deficient MC calls for detailed investigations of the cooperative action of autophagy and Nrf2 in controlling ROS levels in MC biology and human pathologies associated with oxdiative damage. (Schallreuter, 2007;Swalwell *et al.*, 2012)

Materials and methods

Mice and genotyping

Atg7-floxed mice and Tyr::Cre mice have been described previously (Komatsu *et al.*, 2005;Delmas *et al.*, 2003). Tyr::Cre mice were crossed with Atg7-floxed mice to yield Atg7 f/f and Atg7 f/f Tyr::Cre mice housed under specific pathogen-free conditions. Since the Tyr::Cre transgene is located on the X chromosome, all *in vivo* data were derived from Tyr::Cre males to exclude effects of X-chromosome inactivation. For *in vitro* experiments, we further crossed male Atg7 f/f Tyr::Cre mice (Xtg/Y) with female Atg7 f/f hemizygous Tyr::Cre mice (Xtg/Xo) to generate female Atg7 f/f homozygous Tyr::Cre mice (Xtg/Xtg). Those female Atg7 f/f homozygous Tyr::Cre mice (Xtg/Xtg) were then back-crossed with male Atg7 f/f Tyr::Cre mice (Xtg/Y) so that all pups were either Atg7 f/f Tyr::Cre mice (Xtg/Y) or Atg7 f/f homozygous Tyr::Cre mice (Xtg/Xtg), whose Atg7 was specifically knocked out in MC. All mice were maintained in a regular 12 hours light-dark cycle on a normal diet with free access to drinking water. Genotyping by PCR was carried out as described(Colombo *et al.*, 2007).

Human and mouse primary MC culture.

Normal human epidermal melanocytes were obtained from Lonza (Basel, Switzerland) and cultured in melanocyte growth medium (MGM-4, Lonza). Primary mouse MC were prepared from 1-to-5-days old pups as described (Bennett *et al.*, 1989) with slight modifications. Briefly, dorsal skin was washed 3 times with 70% ethanol and sterile PBS for 3 times and fat removed. The skin was then cut into 3-4 small pieces and incubated in 2ml dispase II (Roche, Basel Switzerland 2.4 U/ml) in a 60 mm petri dish at 37°C for 1h. Epidermis was separated from dermis by standard sequential dispase (Roche, 2.4 U/ml) and trypsin/EDTA (Clonetics, 0.25 mg/ml) digestion. Medium containing fetal calf serum was used to stop trypsinization, followed by centrifugation (1500 rpm, 2min). The pellet was resuspended in melanocyte growth medium (MGM-4, Lonza, Basel, Switzerland). Passages were made when cultures became subconfluent and cells were counted at each passage.

Melanin content

Dorsal hair was collected from Atg7 f/f and Atg7 f/f Tyr::Cre (Xtg/Y) male mice in different ages. Melanin from 4mg hair from each mouse was extracted in 1ml NaOH (1 M) at 80°C for 4 h (Guyonneau *et al.*, 2004). For cultured primary mouse MC, cells from Atg7 f/f and Atg7 f/f Tyr::Cre mice((Xtg/Xtg) or (Xtg/Y)) mice were collected by trypsinization and counted. 1 x 10^5 cells from each sample were centrifuged down and washed twice with PBS. The pellet was then incubated in 0.5 ml NaOH (1 M) at

80°C for 1 h. Standard curve covering concentration range of 0-640 µg/ml was generated using synthetic melanin (M8631, Sigma, St. Louis). The absorbance of the supernatants was measured by spectrophotometry at 475 nm and the melanin content is expressed as µg per mg hair or pg per cell. Each hair sample and cell sample was measured in duplicate.

Proliferation assay

Cultured primary MC in aliquots of $5x10^4$ cells were labeled with 10 µM carboxy-fluorescein diacetate succinimidyl ester (CFSE) (Life Technologies, Carlsbad, CA) according to the manufacturer's protocol. After 8 days in culture cells were trypsinized and analyzed by flow cytometry on a FACS Calibur (Becton Dickinson, Mountain View, CA) and data were analyzed using FlowJo software (Tree Star Inc., Ashland, OR).

Immunofluorescence analysis

For the analysis of tyrosinase, p62, p16ink4a, Ki67 and poly-ubiquitin in primary mouse MC, cells from Atg7 f/f and Atg7 f/f Tyr::Cre (Xtg/Y) mice were seeded on a 4-well imaging chamber CG (PAA Laboratories GmbH, Austria) overnight. Cells were then fixed with 4% PFA at room temperature for 10 minutes. Polyclonal rabbit anti p62/SQSTM1 (MBL, Woburn, MA; dilution 1:1000), monoclonal mouse anti p16Ink4a (Santa Cruz, CA, USA, dilution 1:500),monoclonal rat anti Ki-67 (DakoCytomation, Carpinteria, CA, USA, dilution 1:25), monoclonal mouse anti-mono and polyubiquitinylated conjugates (clone FK2, monoclonal mouse, BML-PW8810-0500, Enzo Lifescience, NY, USA, dilution 1:5000) in PBS, pH 7.2, 2% bovine serum albumin (BSA) were applied overnight at 4°C. The samples were then incubated with 10% goat serum (DakoCytomation, Carpinteria, CA, USA) to block non-specific binding of second step antibodies, and finally with goat anti-rabbit and anti-mouse goat antisera conjugated with Alexa Fluor 488 and 546 (Molecular Probes, Leiden, The Netherlands) for 30 minutes. Hoechst 33258 (Molecular Probes) was used to label the nuclei. For the immunofluorescence analysis of tyrosinase and p62 *in vivo*, epidermal sheets from tail skin of Atg7 f/f and Atg7 f/f Tyr::Cre mice were prepared and stained as described before (Tschachler et al., 2004). Briefly, after digestion with 3.8% ammonium thiocyanate solution in PBS at 37°C for 30min, epidermis was separated from dermis and fixed with 4%PFA at 4°C for 30min. Epidermal sheets were then incubated with 10% donkey serum (Abcam, Cambridge, UK,) for 1hr, polyclonal goat anti tyrosinase (Santa Cruz, sc-7834, dilution 1:250) and polyclonal rabbit anti p62/SQSTM1 (MBL, dilution 1:500) overnight at 4°C, and finally with AlexaFluor 546 donkey anti goat IgG and 488 donkey anti rabbit IgG (Molecular Probes) for 1h. Appropriate isotype controls were included and gates were set according to isotype-matched controls. The presence of

tyrosinase, p62, Ki67 and mono- and polyubiquitinylated conjugates staining was investigated using a conventional fluorescence microscope. Tyrosinase and p62 staining in vivo was investigated by laser scanning microscopy (LSM 700) and Zen 2009 software (both Carl Zeiss Jena, Germany). Stacks of images were acquired with a 63× objective (oil immersion) in thickness of 20µm and comprised 20 slices each, spaced by approximately 1µm. For illustration purposes, all images from each stack were projected in to one composite picture.

Western blot analysis

Cultured primary mouse MC were placed in lysis buffer containing 50 mM Tris (pH 7.4), 2% SDS and complete protease inhibitor cocktail (Roche) and sonicated. The insoluble debris was removed by centrifugation and the protein concentration of the supernatant was measured by the BCA (bicinchoninic acid) method (Pierce, Rockford, IL). Western blot analysis was performed as described previously (Sukseree et al., 2012). The following first step antibodies were used for the detection of specific antigens: Rabbit anti-Atg7 (A2856, Sigma, St. Louis, USA, dilution 1:2000), rabbit polyclonal anti-p62 (BML-PW9860-0100, Enzo, NY, USA, dilution 1:2000), rabbit polyclonal anti-LC3 (GTX82986, Irvine, CA, dilution 1:2000), goat polyclonal anti-NQO1 (sc-16464, Santa Cruz, dilution 1:200), goat polyclonal to GSTM1 (ab53942, Abcam, dilution 1:2000), mouse monoclonal anti-Txnrd1 (sc-28321, Santa Cruz, dilution 1:100), rabbit polyclonal anti-HO-1 (ADI-SPA-896, Enzo, dilution 1:1000) and mouse monoclonal anti-GAPDH (HyTest Ltd, Finland, 1:2000). As for secondary antibody, goat anti rabbit IgG (Bio-Rad Laboratories, CA, USA), sheep anti-mouse IgG (NA931V, GE healthcare limited, UK) or rabbit anti-goat IgG (P0049, Dako) was used at 1:10000.

Quantitative RT-PCR analysis

RNA was isolated from cultured cells using the RNeasy 96 system (Life Technologies, Carlsbad, CA), and 900 ng of total RNA were reverse-transcribed with iScript cDNA Synthesis Kit (Biorad; Hercules, CA). Primer sequences are (5'-3'): mm_B2M_f: attcacccccactgagactg; mm_B2M_r: tgctatttctttctgcgtgc; mm_p62_f : ccagtgatgaggagctgaca
mm_p62_r: tgggcacacactgcacttat; mm_p16ink4a_f: tctggagcagcatggagtcc; mm_p16ink4a_r: tcgcagttcgaatctgcacc; mm_p21_f: gtacttcctctgccctgctg; mm_p21_r: tctgcgcttggagtgataga; mm_Hmox1_f: gccaccaaggaggtacacat; mm_Hmox1_r: gcttgttgcgctctatctcc; mm_Nqo1_f: gaagctgcagacctggtgat mm_Nqo1_r: ttctggaaaggaccgttgtc; mm_Gclm_f: tggagcagctgtatcagtgg; mm_Gclm_r: agagcagttctttcgggtca; mm_Gstm1_f: ctcccgactttgacagaagc; mm_Gstm1_r: atgtctgcacggatcctctc. qPCR was

performed using LightCycler 480 and the LightCycler 480 SYBR Green I Master (both Roche). The expression of the target transcripts was normalized to the expression of β-2 microglobulin.

Transmission electron microscopy

Tail skin tissues were collected from Atg7 f/f and Atg7 f/f Tyr::Cre adult mice after perfusion and fixed with ice-cold 4% PFA. Primary mouse MCs from Atg7 f/f and Atg7 f/f Tyr::Cre mice were harvested from 12-well plates by adhesion to Aclar film when they reached 80% confluency. Both skin samples and cells were fixed with 2.5% glutaraldehyde in 0.1M Soerensen phosphate buffer, post-fixed with 2% osmium tetroxide in the same buffer, dehydrated in a graded series of ethanol, and embedded in Agar 100 epoxy resin. Ultra-thin sections were cut at a nominal thickness of 70 nm, post-stained with uranyl acetate and 2% lead citrate and inspected in a FEI Morgagni 268d TEM operated at 80 kV. Images were acquired using an 11 megapixel CCD camera from Olympus SIS.

UVB irradiation

Irradiation was performed with a Waldmann F15 T8 tube (Waldmann Medizintechnik, Villingen-Schwenningen, Germany). Energy output of the UVB (280–320 nm) source, monitored with a Waldmann UV meter was 1.1 mW/cm^2 at a tube to target distance of 30 cm. Melanocytes were irradiated with 20 mJ / cm² of UVB. For each experiment, control MC cultures were treated identically except for the exposure to UV light.

ROS assay

MC were incubated in imaging chambers as described above. Seven hours prior to analysis, cells were either incubated with either 1 µM Rapamycin or 1 mM N-Acetylcysteine (both Sigma), one hour prior to analysis "CellROX Green"(Life Technologies, Carlsbad, CA) reagent was added to the medium according to manufacturer's suggestions. After fixation for 15 minutes in 4% PFA, slides were imaged by laser scanning microscopy (LSM 700) and Zen 2009 software (both Carl Zeiss Jena, Germany), and fluorescence of nuclei to which the ROS - oxidized dye binds was quantified using Image J software (http://rsbweb.nih.gov/ij/).

HPLC MS/MS quantification of oxidized phospholipids.

Analysis of lipids was performed using liquid-liquid extraction procedure followed by quantification using mass spectrometry as described by us recently(Gruber et al., 2012). Cells were washed with PBS followed by addition of cold acidified methanol and internal standard (dinonanoyl-phosphatidylcholine, Avanti,

Alabaster, AL). Neutral lipids and fatty acids were removed by 3 extractions with hexane. Analysis of phospholipids was performed using reversed phase chromatography followed by on-line electrospray ionization-MS/MS procedure as described (Gruber et al., 2012) at FTC-Forensic Toxicological Laboratory, Vienna, Austria.

Conflict of interest

The authors state no conflict of interest.

Acknowledgements

The authors are grateful to Masaaki Komatsu (Tokyo Metropolitan Institute of Medical Science, Tokyo, Japan) for providing Atg7-floxed mice and to Vincent Hearing (NIH) for the kind gift of aPEP7 antibody that was used in preliminary studies. We thank Minoo Ghannadan and Maria Buchberger for technical advice and helpful discussions. We thank Harald Höger for the maintenance of the mice and the Core Facility Imaging of the Medical University of Vienna for excellent technical support. This work was supported by research grants from CE.R.I.E.S, Neuilly, France). The financial support by the Federal Ministry of Science, Research and Economy (BMWFW) and the National Foundation for Research, Technology, and Development is gratefully acknowledged.

Figure legends

Figure 1. Autophagy is constitutively active in normal human and murine MC
Primary human (hMC) and mouse (mMC) melanocytes were subjected to rapamycin treatment at 0.5 ug/ml for 1 h. Cell lysates of rapamycin- treated and untreated cells were subjected to Western blot analysis for LC3 and GAPDH as a loading control. Bands corresponding to LC3-I and LC3-II (indicative of active autophagy) are marked by arrows.

Figure 2. Deletion of Atg7 blocks autophagy in MC from Atg7 f/f Tyr::Cre mice
(a) DNA was prepared from cultured MC from Atg7 f/f and Atg7 f/f Tyr::Cre mice and then subjected to PCR. The diagram on the right shows the deletion of the Atg7 gene by pigment-cell-specific expression of Cre recombinase, using mice carrying a floxed alleles of Atg7 and the Tyr::Cre transgene. (b) Primary MC

isolated from Atg7 f/f and Atg7 f/f Tyr::Cre mice were analyzed by Western blot for Atg7 (upper panel), LC3 (middle panel) and GAPDH (lower panel). Bands corresponding to LC3-I and LC3-II are marked by arrows.

Figure 3. Genetic suppression of autophagy in MC leads to decreased melanin content of dorsal hair but non-significant change of melanin content of primary MC

(a) Left: Representative photograph of the lower backs and tails of an Atg7 f/f and an Atg7 f/f Tyr::Cre mouse at the age of 9 months. Right: enlarged pictures of the tail shafts. (b) Dorsal hair melanin content from Atg7 f/f Tyr::Cre (n=10) and Atg7 f/f mice (n=9) at the age of day 32-35 (5 weeks of age = w5), day 61-64 (w9), day 90-94 (w13), day 118-124 (w18) and day 177-182 (w26). (c) Primary autophagy-deficient and autophagy-competent MC were isolated from body skin of newborn mice of the respective mouse strains and cultured *in vitro* under identical conditions and analysed at days 12, 24 and 36 for their melanin content (individual cultures; n=3).

Figure 4. Autophagy deficiency leads to decreased proliferation and premature senescence in cultured primary MC (a) Proliferation of Atg7 f/f and Atg7 f/f Tyr::Cre cells, passage number plotted against days in culture. (b) Immunofluorescence analysis of Ki67 expression (red) in the MC from Atg7 f/f and Atg7 f/f Tyr::Cre mice. Bar=10 μm and (c) quantification (n=5). (d) Representative photos of MC from Atg7 f/f and Atg7 f/f Tyr::Cre mice at the age of day 8, day 24, day 36 and day 65. Phase contrast micrographs, bar=250 μm. (e) Primary autophagy-deficient and competent MC were cultured for 22 days and expression of p16Ink4a and p21 were determined using qPCR (n=3; relative quantification, normalized to expression of beta-2-microglobulin; error bars indicate ± SD * indicates $P<0.05$ (*t*-test). (f,g) Primary autophagy-deficient and competent MC were cultured for 22 days, sham irradiated or irradiated with 20 mJ / cm² of UVB and subjected to immunofluorescent staining for p16Ink4a. Bar=10 μm (g) The percentage of p16Ink4a positive nuclei was determined in three independent cultures (n=3) for each genotype and treatment (error bars indicate ± SD ; * indicates $P<0.05$ (*t*-test)).

Figure 5. Autophagy deficiency leads to accumulation of high molecular weight protein aggregates containing p62.

(a) Lysates of primary MC from Atg7 f/f and Atg7 f/f Tyr::Cre mice were subjected to Western blot analysis for p62. (b) Immunofluorescence analysis for p62 (green) and (poly-)ubiquitinated protein (red) in MC isolated from Atg7 f/f and Atg7 f/f Tyr::Cre mice. Bar=10 μm. (c) Epidermal sheet preparations

were stained for Tyrosinase (red), p62(green), nuclei (blue) and analyzed by laser scanning microscopy. Bar=10 μm.

(d) Primary autophagy-deficient and autophagy-competent MC were cultured for 22 days and subjected to qPCR for p62. Error bars represent mean ± SD across three independent cultures (n=3). **: P<0.01. (*t*-test)

Figure 6. Autophagy deficiency leads to enhanced expression of Nrf2 target genes but also to increased phospholipid oxidation.

(a) Primary autophagy-deficient and autophagy-competent MC were cultured for 22 days and subjected to qPCR for Hmox-1, Nqo-1, Gclm, and Gstm1. Error bars represent mean ± SD (n=3) and *t*-test was performed. **: P<0.01; *: P<0.05; n.s.: non-significant difference. (b) Lysates of primary MC from Atg7 f/f and Atg7 f/f Tyr::Cre mice were subjected to Western blot analysis for NQO-1, GSTM1, HO-1 and GAPDH. (c) Primary autophagy-deficient and autophagy-competent MC were cultured for 22 days. Relative amounts of PLPC and SLPC hydroperoxides relative to their unoxidized precursors and amount of DPPC relative to PLPC were quantified using HLPC-MS/MS. The data are presented as normalized peak intensities in autphagy deficient cells compared to autophagy competent MCs. Error bars indicate standard deviations within biological triplicates. Asterisks indicate significant differences (*P<0.05), gray bars indicate Atg7 f/f Tyr::Cre in (a) and (c) .

Supplementary material

Supplementary Figure S1. Melanocyte counts in Atg7 f/f and Atg7 f/f Tyr::Cre

Five milimeter punches were prepared from whole tail skin of both genotypes (for each n=5) and epidermis was separated from dermis by incubation on 3,8% ammonium thiocyanate, 3/°C, 30 minutes. Epidermis was fixed for 30 minutes in 5% formalin at 4°C. Samples were washed and stained with DOPA for 18 hours at 37°C in the dark according to (Laidlaw and Blackberg, 1932), and mounted on glass slides. The numbers of melanocytes per punch were imaged, counted and normalized to total pixel area with ImageJ to compensate for variations in punch size. Counts were averaged from 3 independent observers blinded to the genotype of the mice.

Supplementary Figure S2. Atg7 f/f Tyr::Cre can form mature melanosomes that are transferred to keratinocytes.

(a, b) Electron micrographs of skin sections from Atg7 f/f (a) and Atg7 f/f Tyr::Cre (b) mice. Melanin granules are visible in the stratum corneum (Sc) of autophagy competent and autophagy deficient mice. (c, d) High power electron micrographs of epidermal melanocytes *in situ. (*c) White arrows represent stage VI eumelanosomes with intact granule delimiting membranes. (d) White arrows represent stage VI

eumelanosomes with swollen melanin granule delimiting membranes (arrowhead). Black arrows show fragmented membrane of a swollen mitochondrion. (e-h) Electron micrographs of cultured melanocytes from Atg7 f/f (e) and Atg7 f/f Tyr::Cre (f) mice. Black frames indicate the position of the high power details in (g) and (h). (g) Black arrows represent stage VI eumelanosomes. White arrows represent immature pre-melanosomes. (h) Black arrows represent stage VI eumelanosomes. White arrows represent immature pre-melanosomes. Several melanosomes exhibit swollen delimiting membranes.
Abbreviation key: Mt = mitochondria; Nu = Nuclei; Epi = Epidermis; Der = Dermis; Sc = Stratum corneum.

Supplementary Figure S3. Nrf2 expression

Primary autophagy-deficient and autophagy-competent MC were cultured for 22 days and relative Nrf2 mRNA expression were quantified by qPCR. Relative expression shown normalized to B2M. n.s denotes non significant difference. Error bars represent ± SD (n=3)

Supplementary Figure S4. ROS assay

MC were cultured in imaging chambers at day 22. Seven hours prior to analysis, cells were either incubated with either Rapamycin 1µM or N-Acetylcysteine 1mM and one hour prior to analysis "CellROX Green" reagent was added to the medium. Fluorescence intensity of nuclei, where the ROS modified dye binds to DNA was quantified from laser scanning microscope files using ImageJ software. Three replicates per condition with at least 30 nuclei were quantified, error bars represent mean fluorescence intensities +/- SD, asterisks indicate significant differences (*P<0.05).

Reference List

Bellei B, Pitisci A, Ottaviani M et al. (2013) Vitiligo: a possible model of degenerative diseases. ***PLoS One*** **8: e59782.**

Bennett DC, Cooper PJ, Dexter TJ et al. (1989) Cloned mouse melanocyte lines carrying the germline mutations albino and brown: complementation in culture. ***Development*** **105: 379-385.**

Bonaventure J, Domingues MJ, Larue L (2013) Cellular and molecular mechanisms controlling the migration of melanocytes and melanoma cells. ***Pigment Cell Melanoma Res*** **26: 316-325.**

Colombo S, Petit V, Kumasaka M et al. (2007) Flanking genomic region of Tyr::Cre mice, rapid genotyping for homozygous mice. ***Pigment Cell Res*** **20: 305-306.**

Dell'Anna ML, Ottaviani M, Bellei B et al. (2010) Membrane lipid defects are responsible for the generation of reactive oxygen species in peripheral blood mononuclear cells from vitiligo patients. ***J Cell Physiol*** **223: 187-193.**

Delmas V, Martinozzi S, Bourgeois Y et al. (2003) Cre-mediated recombination in the skin melanocyte lineage. ***Genesis*** **36: 73-80.**

Deretic V (2011) Autophagy in immunity and cell-autonomous defense against intracellular microbes. ***Immunol Rev*** **240: 92-104.**

Funderburk SF, Wang QJ, Yue Z (2010) The Beclin 1-VPS34 complex--at the crossroads of autophagy and beyond. ***Trends Cell Biol*** **20: 355-362.**

Ganesan AK, Ho H, Bodemann B et al. (2008) Genome-wide siRNA-based functional genomics of pigmentation identifies novel genes and pathways that impact melanogenesis in human cells. ***PLoS Genet*** **4: e1000298.**

Girotti AW (1998) Lipid hydroperoxide generation, turnover, and effector action in biological systems. ***J Lipid Res*** **39: 1529-1542.**

Girotti AW, Kriska T (2004) Role of lipid hydroperoxides in photo-oxidative stress signaling. ***Antioxid Redox Signal*** **6: 301-310.**

Gruber F, Bicker W, Oskolkova OV et al. (2012) A simplified procedure for semi-targeted lipidomic analysis of oxidized phosphatidylcholines induced by UVA irradiation. ***J Lipid Res*** **53: 1232-1242.**

Guo JL, Lee VM (2014) Cell-to-cell transmission of pathogenic proteins in neurodegenerative diseases. ***Nat Med*** **20: 130-138.**

Guyonneau L, Murisier F, Rossier A et al. (2004) Melanocytes and pigmentation are affected in dopachrome tautomerase knockout mice. ***Mol Cell Biol*** **24: 3396-3403.**

Hearing VJ (1993) Unraveling the melanocyte. ***Am J Hum Genet*** **52: 1-7.**

Hirobe T (1984) Histochemical survey of the distribution of the epidermal melanoblasts and melanocytes in the mouse during fetal and postnatal periods. ***Anat Rec*** **208: 589-594.**

Hirobe T (2011) How are proliferation and differentiation of melanocytes regulated? ***Pigment Cell Melanoma Res*** **24: 462-478.**

Ho H, Ganesan AK (2011) The pleiotropic roles of autophagy regulators in melanogenesis. *Pigment Cell Melanoma Res* 24: 595-604.

Ichimura Y, Waguri S, Sou YS et al. (2013) Phosphorylation of p62 activates the Keap1-Nrf2 pathway during selective autophagy. *Mol Cell* 51: 618-631.

Inoue D, Kubo H, Taguchi K et al. (2011) Inducible disruption of autophagy in the lung causes airway hyper-responsiveness. *Biochem Biophys Res Commun* 405: 13-18.

Jain A, Lamark T, Sjottem E et al. (2010) p62/SQSTM1 is a target gene for transcription factor NRF2 and creates a positive feedback loop by inducing antioxidant response element-driven gene transcription. *J Biol Chem* 285: 22576-22591.

Jian Z, Li K, Song P et al. (2014) Impaired Activation of the Nrf2-ARE Signaling Pathway Undermines H2O2-Induced Oxidative Stress Response: A Possible Mechanism for Melanocyte Degeneration in Vitiligo. *J Invest Dermatol* 134: 2221-2230.

Kalie E, Razi M, Tooze SA (2013) ULK1 regulates melanin levels in MNT-1 cells independently of mTORC1. *PLoS One* 8: e75313.

Kang HT, Lee KB, Kim SY et al. (2011) Autophagy impairment induces premature senescence in primary human fibroblasts. *PLoS One* 6: e23367.

Kim ES, Chang H, Choi H et al. (2014) Autophagy induced by resveratrol suppresses alpha-MSH-induced melanogenesis. *Exp Dermatol* 23: 204-206.

Kirkin V, Lamark T, Sou YS et al. (2009) A role for NBR1 in autophagosomal degradation of ubiquitinated substrates. ***Mol Cell*** **33: 505-516.**

Kobayashi M, Yamamoto M (2005) Molecular mechanisms activating the Nrf2-Keap1 pathway of antioxidant gene regulation. ***Antioxid Redox Signal*** **7: 385-394.**

Kokot A, Metze D, Mouchet N et al. (2009) Alpha-melanocyte-stimulating hormone counteracts the suppressive effect of UVB on Nrf2 and Nrf-dependent gene expression in human skin. ***Endocrinology*** **150: 3197-3206.**

Komatsu M, Kurokawa H, Waguri S et al. (2010) The selective autophagy substrate p62 activates the stress responsive transcription factor Nrf2 through inactivation of Keap1. ***Nat Cell Biol*** **12: 213-223.**

Komatsu M, Waguri S, Chiba T et al. (2006) Loss of autophagy in the central nervous system causes neurodegeneration in mice. ***Nature*** **441: 880-884.**

Komatsu M, Waguri S, Ueno T et al. (2005) Impairment of starvation-induced and constitutive autophagy in Atg7-deficient mice. ***J Cell Biol*** **169: 425-434.**

Laidlaw GF, Blackberg SN (1932) Melanoma Studies: II. A Simple Technique for the Dopa Reaction. ***Am J Pathol*** **8: 491-498.**

Lionaki E, Markaki M, Tavernarakis N (2013) Autophagy and ageing: insights from invertebrate model organisms. ***Ageing Res Rev*** **12: 413-428.**

Luciani F, Champeval D, Herbette A et al. (2011) Biological and mathematical modeling of melanocyte development. *Development* 138: 3943-3954.

Marrot L, Jones C, Perez P et al. (2008) The significance of Nrf2 pathway in (photo)-oxidative stress response in melanocytes and keratinocytes of the human epidermis. *Pigment Cell Melanoma Res* 21: 79-88.

Mizushima N (2007) Autophagy: process and function. *Genes Dev* 21: 2861-2873.

Mizushima N, Komatsu M (2011) Autophagy: renovation of cells and tissues. *Cell* 147: 728-741.

Mizushima N, Levine B (2010) Autophagy in mammalian development and differentiation. *Nat Cell Biol* 12: 823-830.

Murase D, Hachiya A, Takano K et al. (2013) Autophagy has a significant role in determining skin color by regulating melanosome degradation in keratinocytes. *J Invest Dermatol* 133: 2416-2424.

Natarajan VT, Singh A, Kumar AA et al. (2010) Transcriptional upregulation of Nrf2-dependent phase II detoxification genes in the involved epidermis of vitiligo vulgaris. *J Invest Dermatol* 130: 2781-2789.

Pankiv S, Clausen TH, Lamark T et al. (2007) p62/SQSTM1 binds directly to Atg8/LC3 to facilitate degradation of ubiquitinated protein aggregates by autophagy. *J Biol Chem* 282: 24131-24145.

Piepkorn M (2000) The expression of p16(INK4a), the product of a tumor suppressor gene for melanoma, is upregulated in human melanocytes by UVB irradiation. *J Am Acad Dermatol* 42: 741-745.

Puig I, Yajima I, Bonaventure J et al. (2009) The tyrosinase promoter is active in a subset of vagal neural crest cells during early development in mice. *Pigment Cell Melanoma Res* 22: 331-334.

Riley BE, Kaiser SE, Shaler TA et al. (2010) Ubiquitin accumulation in autophagy-deficient mice is dependent on the Nrf2-mediated stress response pathway: a potential role for protein aggregation in autophagic substrate selection. *J Cell Biol* 191: 537-552.

Rossiter H, Konig U, Barresi C et al. (2013) Epidermal keratinocytes form a functional skin barrier in the absence of Atg7 dependent autophagy. *J Dermatol Sci* 71: 67-75.

Sanchez CG, Penfornis P, Oskowitz AZ et al. (2011) Activation of autophagy in mesenchymal stem cells provides tumor stromal support. *Carcinogenesis* 32: 964-972.

Santambrogio L, Cuervo AM (2011) Chasing the elusive mammalian microautophagy. *Autophagy* 7: 652-654.

Schafer M, Farwanah H, Willrodt AH et al. (2012) Nrf2 links epidermal barrier function with antioxidant defense. *EMBO Mol Med* 4: 364-379.

Schallreuter KU (2007) Advances in melanocyte basic science research. *Dermatol Clin* 25: 283-91, vii.

Sena LA, Chandel NS (2012) Physiological roles of mitochondrial reactive oxygen species. *Mol Cell* 48: 158-167.

Singh SK, Kurfurst R, Nizard C et al. (2010) Melanin transfer in human skin cells is mediated by filopodia--a model for homotypic and heterotypic lysosome-related organelle transfer. *FASEB J* 24: 3756-3769.

Slominski A, Paus R (1993) Melanogenesis is coupled to murine anagen: toward new concepts for the role of melanocytes and the regulation of melanogenesis in hair growth. ***J Invest Dermatol*** **101: 90S-97S.**

Slominski A, Wortsman J, Plonka PM et al. (2005) Hair follicle pigmentation. ***J Invest Dermatol*** **124: 13-21.**

Swalwell H, Latimer J, Haywood RM et al. (2012) Investigating the role of melanin in UVA/UVB- and hydrogen peroxide-induced cellular and mitochondrial ROS production and mitochondrial DNA damage in human melanoma cells. ***Free Radic Biol Med*** **52: 626-634.**

Tschachler E, Reinisch CM, Mayer C et al. (2004) Sheet preparations expose the dermal nerve plexus of human skin and render the dermal nerve end organ accessible to extensive analysis. ***J Invest Dermatol*** **122: 177-182.**

van Schanke A., Jongsma MJ, Bisschop R et al. (2005) Single UVB overexposure stimulates melanocyte proliferation in murine skin, in contrast to fractionated or UVA-1 exposure. ***J Invest Dermatol*** **124: 241-247.**

Vellai T (2009) Autophagy genes and ageing. ***Cell Death Differ*** **16: 94-102.**

Yang Z, Klionsky DJ (2010) Mammalian autophagy: core molecular machinery and signaling regulation. ***Curr Opin Cell Biol*** **22: 124-131.**

Zhao Y, Zhang CF, Rossiter H et al. (2013) Autophagy is induced by UVA and promotes removal of oxidized phospholipids and protein aggregates in epidermal keratinocytes. ***J Invest Dermatol*** **133: 1629-1637.**

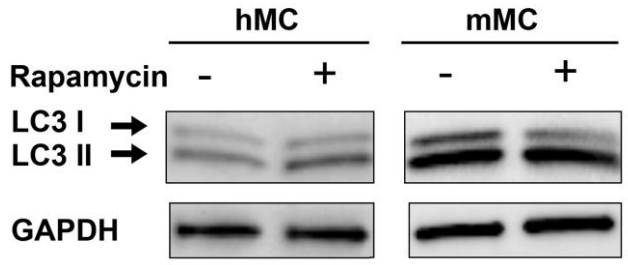

Figure 1

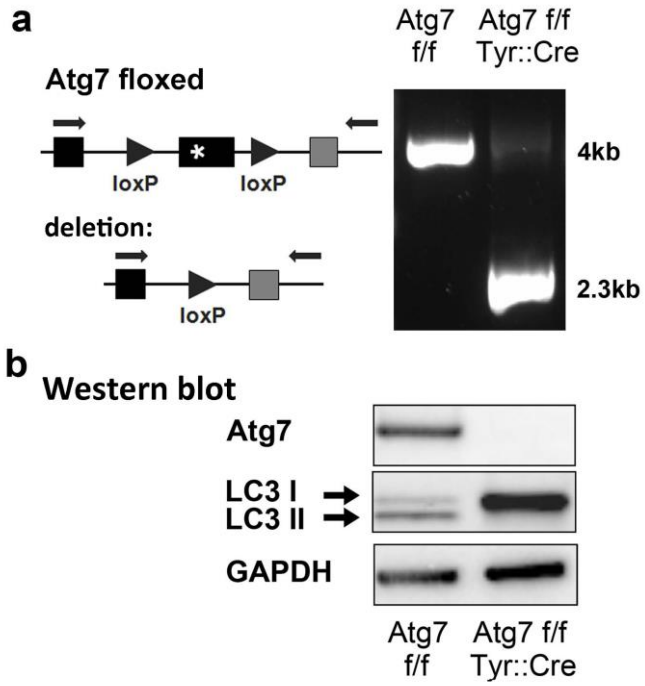

Figure 2

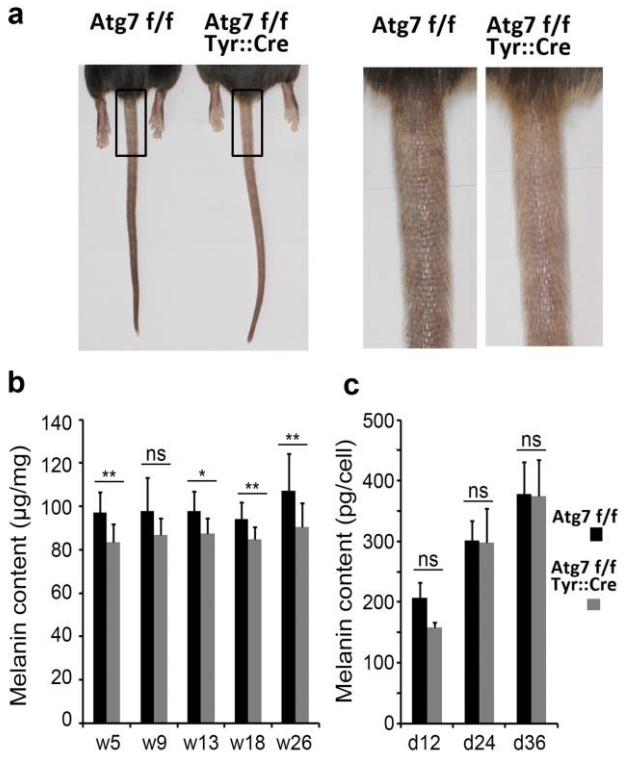
a
Atg7 f/f
Atg7 f/f Tyr::Cre
Atg7 f/f
Atg7 f/f Tyr::Cre
b
Melanin content (µg/mg)
140
120
100
80
60
40
20
0
**
ns
*
**
**
w5
w9
w13
w18
w26
c
Melanin content (pg/cell)
500
400
300
200
100
0
ns
ns
ns
d12
d24
d36
Atg7 f/f
Atg7 f/f Tyr::Cre

Figure 3

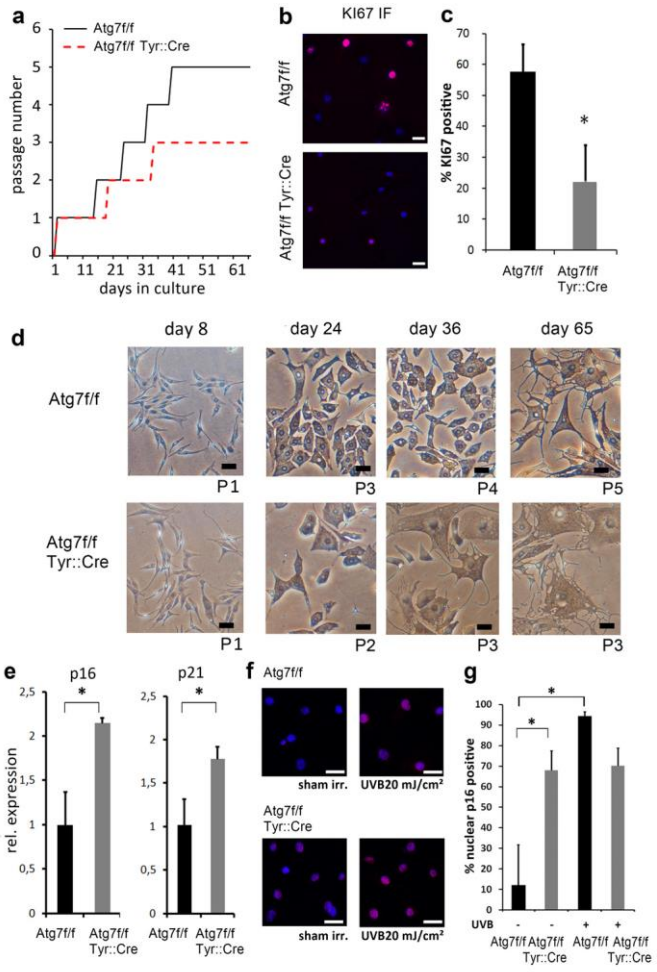
a
Atg7f/f
Atg7f/f Tyr::Cre
passage number
days in culture
b
KI67 IF
Atg7f/f
Atg7f/f Tyr::Cre
c
% KI67 positive
Atg7f/f
Atg7f/f Tyr::Cre
d
day 8
day 24
day 36
day 65
Atg7f/f
Atg7f/f Tyr::Cre
P1
P3
P4
P5
P2
e
p16
p21
rel. expression
f
Atg7f/f
sham irr.
UVB20 mJ/cm²
Atg7f/f Tyr::Cre
g
% nuclear p16 positive
UVB

Figure 4

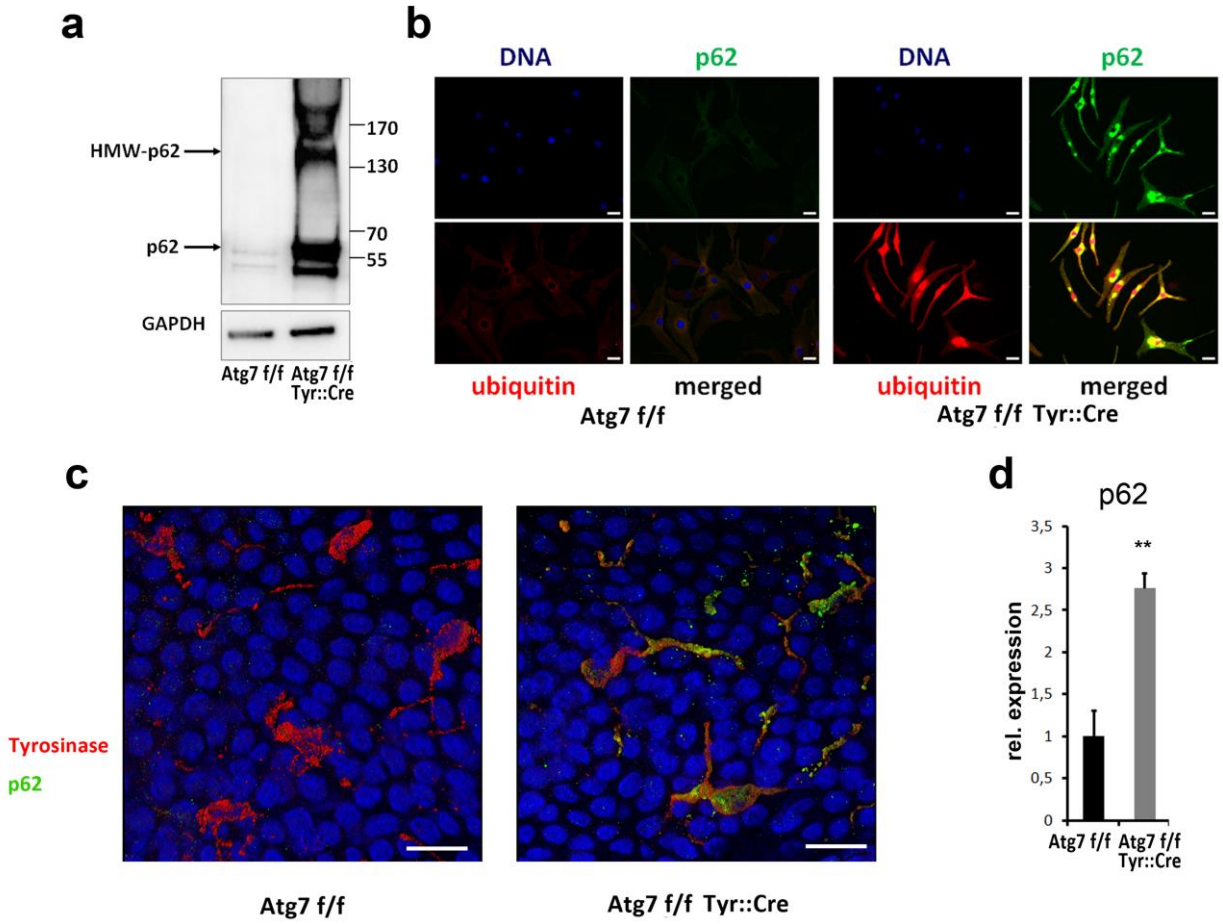
a
HMW-p62
p62
GAPDH
170
130
70
55
Atg7 f/f
Atg7 f/f Tyr::Cre
b
DNA
p62
DNA
p62
ubiquitin
merged
ubiquitin
merged
Atg7 f/f
Atg7 f/f Tyr::Cre
c
Tyrosinase
p62
Atg7 f/f
Atg7 f/f Tyr::Cre
d
p62
rel. expression
**
3,5
3
2,5
2
1,5
1
0,5
0
Atg7 f/f
Atg7 f/f Tyr::Cre

Figure 5

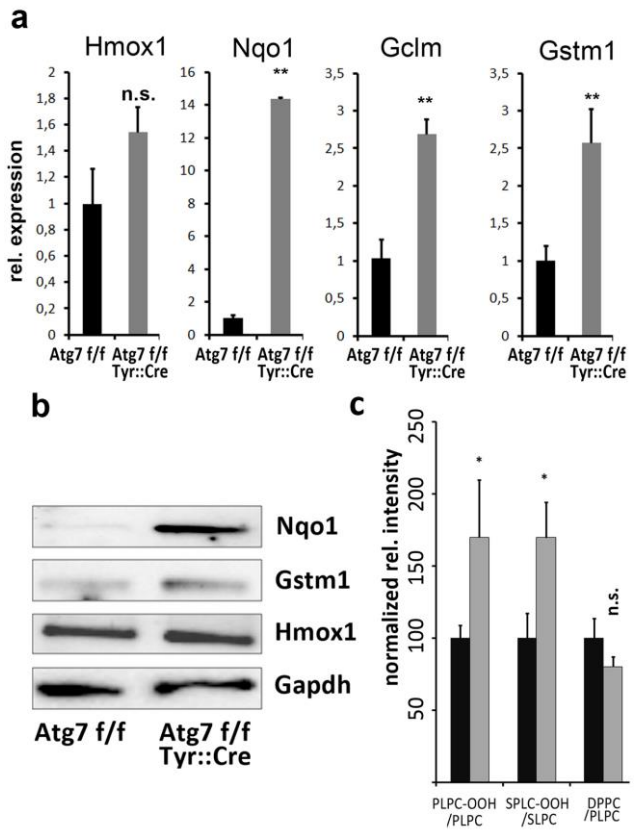
a
Hmox1
Nqo1
Gclm
Gstm1
rel. expression
n.s.
**
**
**
Atg7 f/f
Atg7 f/f Tyr::Cre
b
Nqo1
Gstm1
Hmox1
Gapdh
Atg7 f/f
Atg7 f/f Tyr::Cre
c
normalized rel. intensity
*
*
n.s.
PLPC-OOH /PLPC
SPLC-OOH /SLPC
DPPC /PLPC

Figure 6

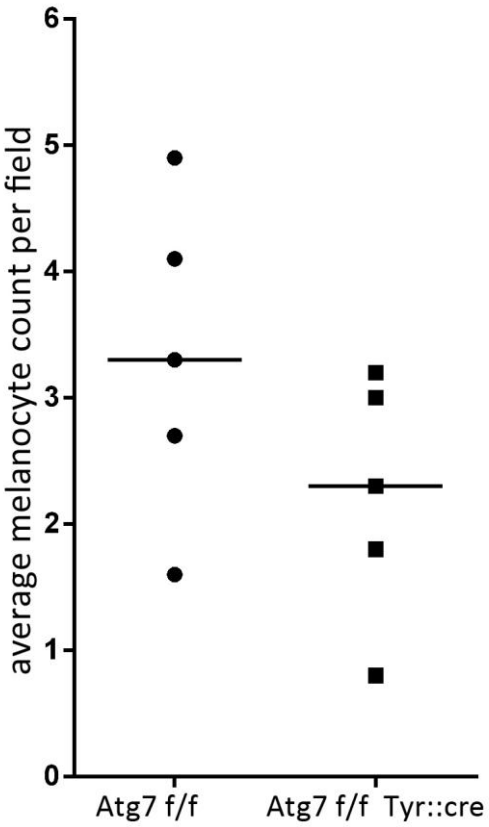

Suppl Figure 1

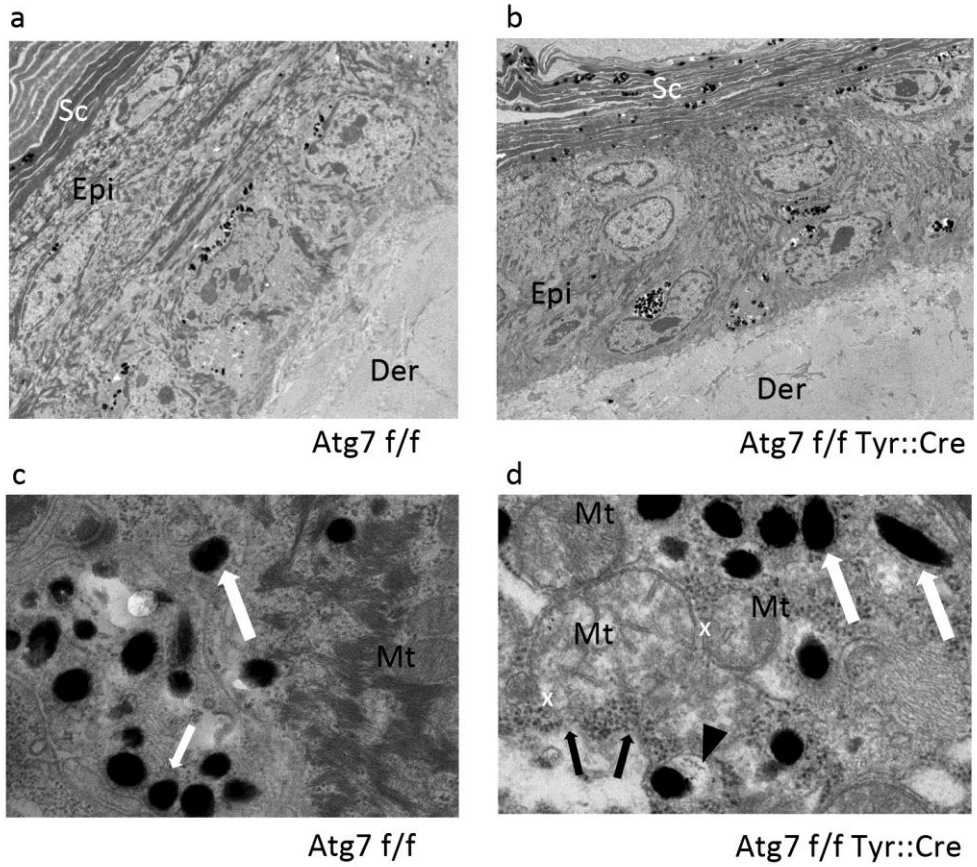

Suppl Figure 2

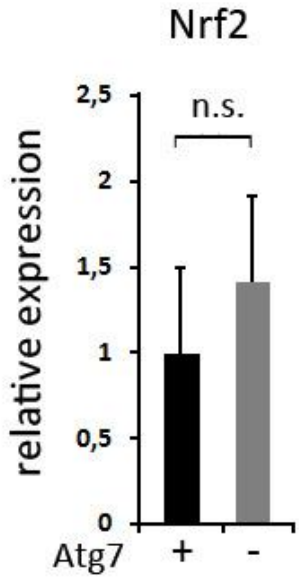

Suppl Figure 3

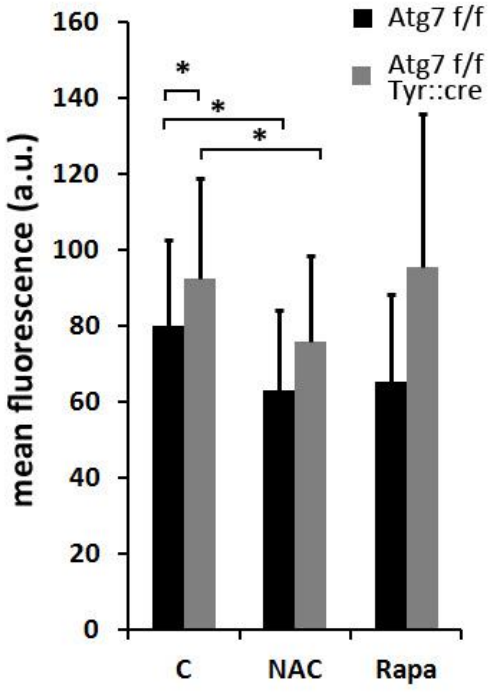

Suppl Figure 4